

Characterization of $Ce_{(1-x)}Zr_xO_2$ yellow nanopigments synthesized by a green sol-gel method



M.S. Nouri^a, A. Kompany^{a,b,*}, A. Khorsand Zak^c, Gh. H. Khorrami^d

^a Electroceramics and Materials Laboratory, Department of Physics, Ferdowsi University of Mashhad, Mashhad, Iran

^b Nano Research Center, Ferdowsi University of Mashhad, Mashhad, Iran

^c Nanotechnology Laboratory, Department of Physics, Esfarayen University of Technology, Iran

^d Department of Physics, Faculty of Basic Science, University of Bojnord, Iran

ARTICLE INFO

Keywords:

$Ce_{(1-x)}Zr_xO_2$

Sol-gel

Yellow nanopigments

ABSTRACT

In this paper, we report on the synthesis of $Ce_{(1-x)}Zr_xO_2$ yellow nanopigments (NPs) by a simple green sol-gel method, using gelatin as the stabilization and polymerization agent. Thermogravimetric analysis (TGA) was employed to obtain the optimum gel calcination temperature. The synthesized $Ce_{(1-x)}Zr_xO_2$ powders were characterized by X-ray diffraction (XRD), Raman spectroscopy, transmission electron microscopy (TEM), UV–vis spectroscopy and CIE-L*a*b* measurement. The XRD patterns of the samples calcined at 600 °C revealed the formation of the desired crystal structures without any secondary phases, confirmed by Raman analysis. The TEM images indicated that the pigments' particle shapes are almost spherical with average particle size of about 8 nm. It was found that by increasing Zr^{+4} concentrations the absorption edge of the produced NPs have a red-shift. The produced NPs had brilliant yellow colour, derived from CIE-L*a*b* coordinates.

1. Introduction

Pigments are generally insoluble, organic or inorganic, powders having varieties of applications including surface coating and colouring other materials such as: ink, plastics, ceramics, cosmetics and food [1–3]. It has been reported that using nanopigments enhances the chemical and mechanical properties and improves the performance of coatings, abrasion resistance, anticorrosion and hardness [4]. There has been great interest in developing highly crystalline, chemically stable and reproducible inorganic NPs such as $Bi_{1-x-y}Ca_xZn_yVO_{4-(x+y)/2}$, $Ni_{0.1}W_{0.1}Ti_{0.8}O_2$, $Ce(MoO_4)_2$ and $(Ca,La)Ta(O,N)_3$ which have been employed for surface coating [5–8]. These pigments, because of their low toxicity, are good candidates to substitute the pigments that contain heavy metals such as: Cd, Co, Cr, Se, Hg and Pb, which are harmful to human health and the environment [8–10]. Furthermore, the use of high-performance organic pigments are limited because of their thermal instability [11]. Pigments based on cerium oxide have been found to give yellow tinge with excellent thermal and chemical stability [3,12]. The colour mechanism of CeO_2 can be modified by doping with some suitable elements, which introduce an additional electronic level between the top of the (O_{2p}) valence band and the bottom of the (Ce_{4f}) conduction band [3]. It has been reported that adding Zr to CeO_2 improves its structural features as well as its thermal

stability. The non-toxic ceria-zirconia compositions have been used as catalysts and also in fabricating fuel cells and oxygen gas sensors [13–15]. The crystal structures of these compounds are monoclinic, tetragonal or cubic depending on the Ce/Zr ratio, calcination temperature and the particle size [16,17].

In this work, environmentally friendly yellow nanopigments based on CeO_2 - ZrO_2 solid solution with the general formula $Ce_{(1-x)}Zr_xO_2$ ($x=0.0, 0.2, 0.4, 0.6, 0.8$) were synthesized by a green sol-gel method. The structural and optical properties of the produced samples have been studied and their colours were investigated quantitatively.

2. Experimental

2.1. Material and methods

The starting materials, used for the synthesis of $Ce_{(1-x)}Zr_xO_2$ nanopowders, were cerium nitrate hexahydrate, $Ce(NO_3)_3 \cdot 6H_2O$, (99% purity, Merck) and zirconium(IV) oxynitrate hydrate, $ZrO(NO_3)_2 \cdot xH_2O$, (99% purity, Sigma-Aldrich). Gelatin type B, from bovine skin (Sigma-Aldrich), was used as the stabilization and polymerization agent and distilled water as the solvent. To obtain 5 g of $Ce_{(1-x)}Zr_xO_2$, certain amounts of cerium and zirconium nitrates were dissolved in 30 ml distilled water, separately. Meanwhile, 10 g of

* Corresponding author at: Electroceramics and Materials Laboratory, Department of Physics, Ferdowsi University of Mashhad, Mashhad, Iran.
E-mail address: kompany@um.ac.ir (A. Kompany).

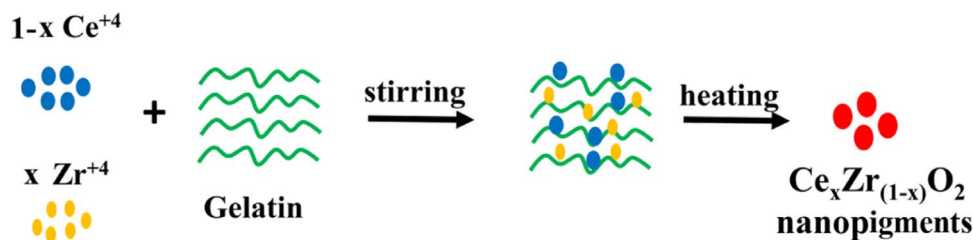


Fig. 1. Schematic diagram of modified sol-gel mechanism for the synthesis of $\text{Ce}_x\text{Zr}_{(1-x)}\text{O}_2$ NPs.



Fig. 2. Photographs of the produced $\text{Ce}_x\text{Zr}_{(1-x)}\text{O}_2$ nanoparticles.

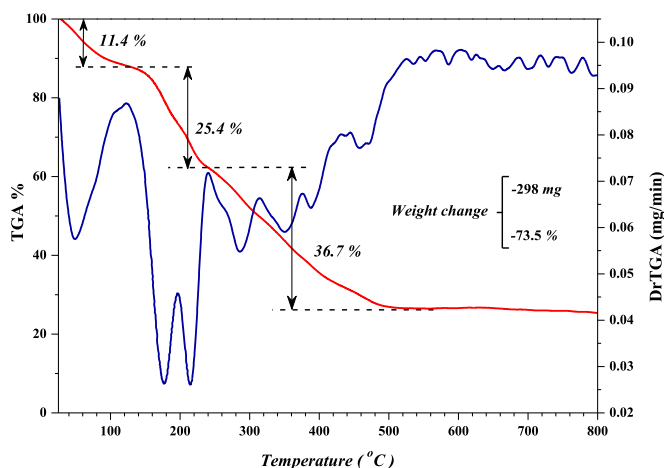


Fig. 3. TGA diagram and the corresponding derivative of the prepared CeO_2 gel.

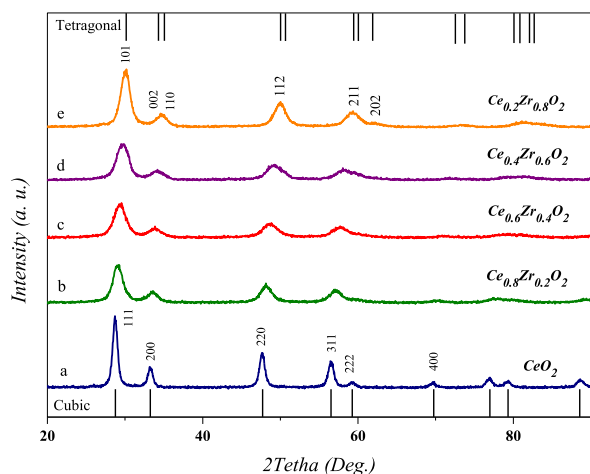


Fig. 4. The XRD patterns of the synthesized samples, (a, b, c) cubic phase, (d, e) tetragonal phase.

gelatin was dissolved in 50 ml of distilled water at 40–50 °C. Then, the two cation solutions were added gradually to the gelatin solution, keeping the temperature at 80 °C. The prepared gel was calcined at 600 °C for 4 h. Fig. 1 shows the preparation procedure of $\text{Ce}_{(1-x)}\text{Zr}_x\text{O}_2$ NPs. The photographs of the final products are presented in Fig. 2.

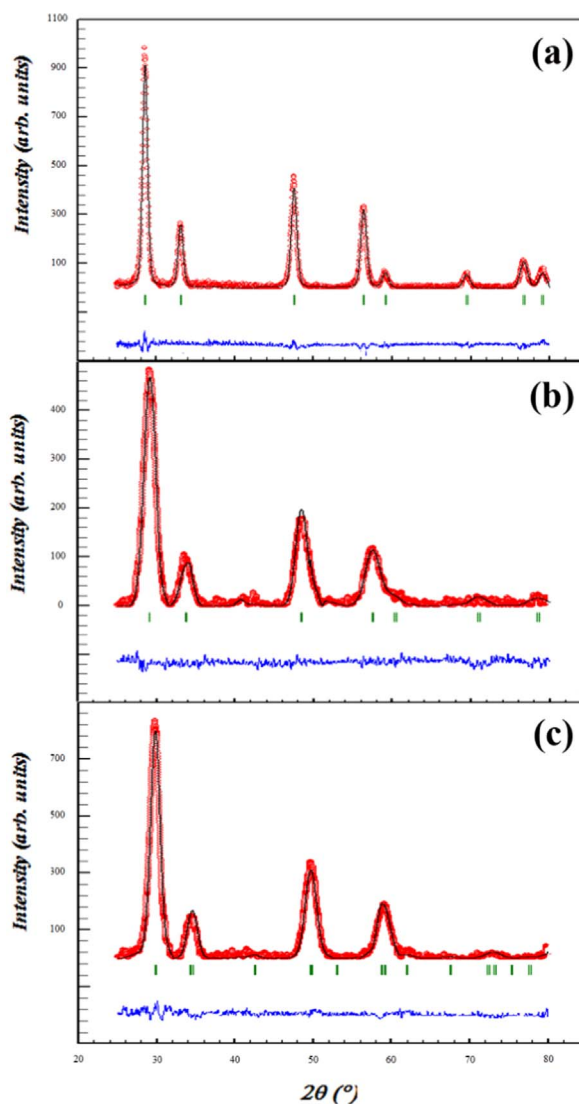


Fig. 5. The XRD refinements of a) CeO_2 , b) $\text{Ce}_{0.6}\text{Zr}_{0.4}\text{O}_2$ and c) $\text{Ce}_{0.2}\text{Zr}_{0.8}\text{O}_2$ NPs.

2.2. Characterizations

In order to determine the optimum calcination temperature, the prepared dried gel was analyzed by thermogravimetric (DTG-60/60,

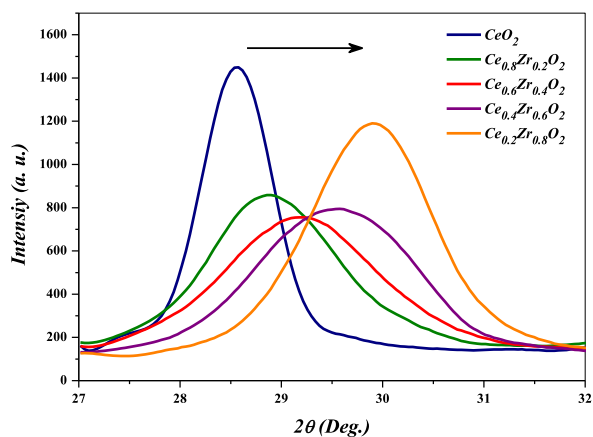


Fig. 6. The main XRD peaks of the prepared $Ce_xZr_{(1-x)}O_2$ NPs.

Table 1

Geometrical parameters of the synthesized $Ce_xZr_{1-x}O_2$.

Compound	Lattice parameter (nm)	Structure	Scherrer formula	SSP method	
			D (nm)	D (nm)	$\epsilon \times 10^{-5}$
CeO_2	a=5.414	Cubic	11.48	10.50	0.25
$Ce_{0.8}Zr_{0.2}O_2$	a=5.388	Cubic	6.15	6.17	1.25
$Ce_{0.6}Zr_{0.4}O_2$	a=5.314	Cubic	4.85	4.99	2.5
$Ce_{0.4}Zr_{0.6}O_2$	a=3.720 c/a=1.42	Tetragonal	5.10	4.99	7.5
$Ce_{0.2}Zr_{0.8}O_2$	a=3.659 c/a=1.43	Tetragonal	6.14	5.72	5

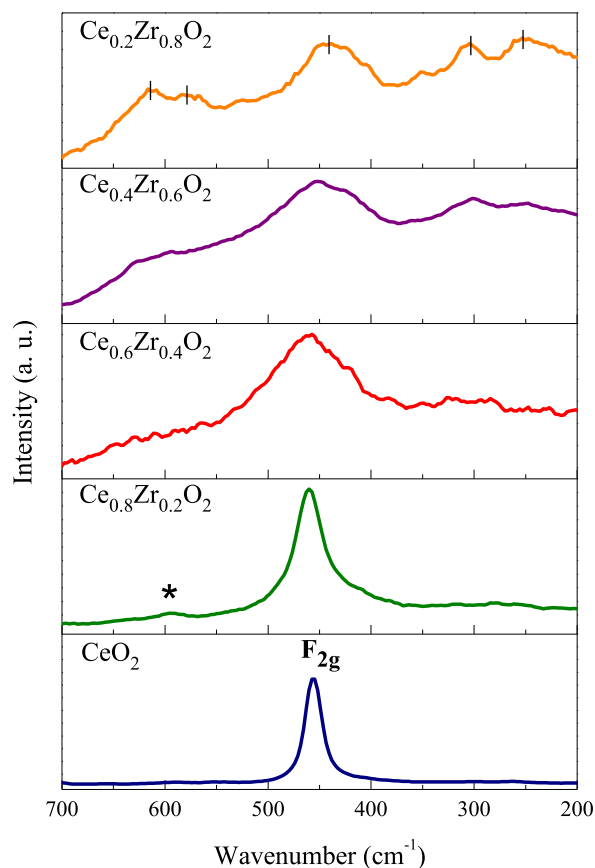


Fig. 8. The Raman Spectra of the synthesized samples.

Shimadzu) technique. The lattice structures of the synthesized samples were investigated by X-ray diffraction (XRD, Philips, X'pert, CuK α), using the Rietveld method, and Raman spectroscopy (AvaSpec-ULS-TEC). Morphology of the prepared samples was examined using

transmission electron microscopy (TEM, CM120, Philips). UV–vis spectroscopy (Jasco, V-670) was employed to determine the value of the optical energy band gap. The CIEL*a*b* colour measurement was

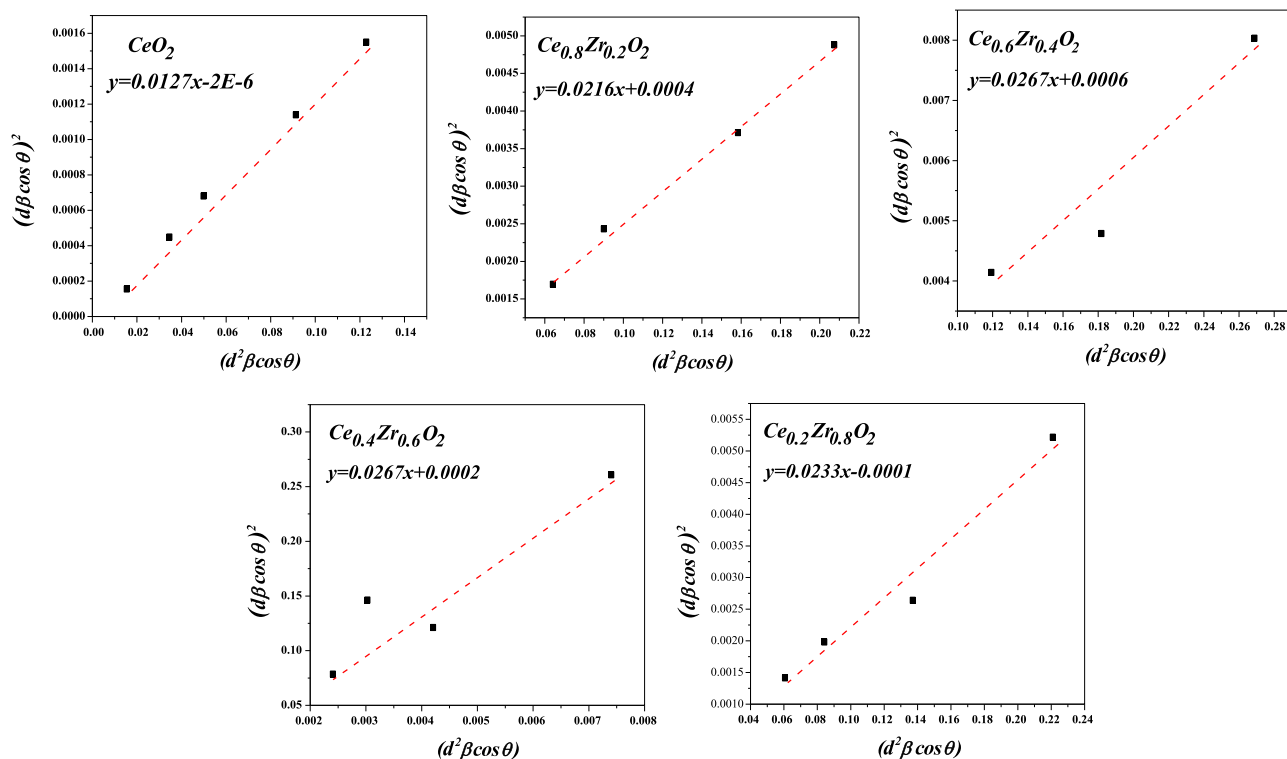


Fig. 7. The SSP plots of the prepared samples.

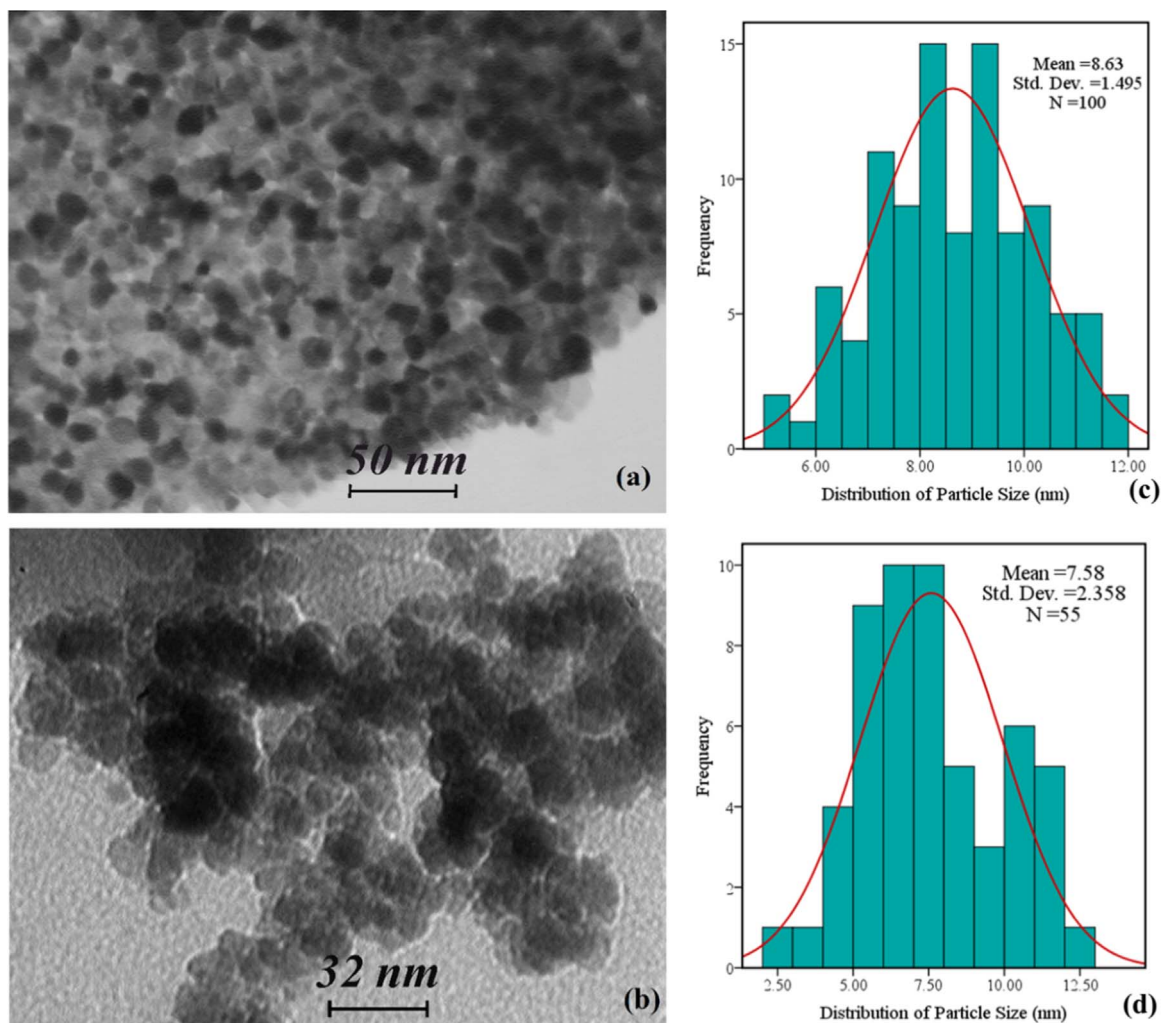


Fig. 9. The TEM micrographs and the corresponding histograms of (a, c) CeO₂ and (b, d) Ce_{0.4}Zr_{0.6}O₂ specimen.

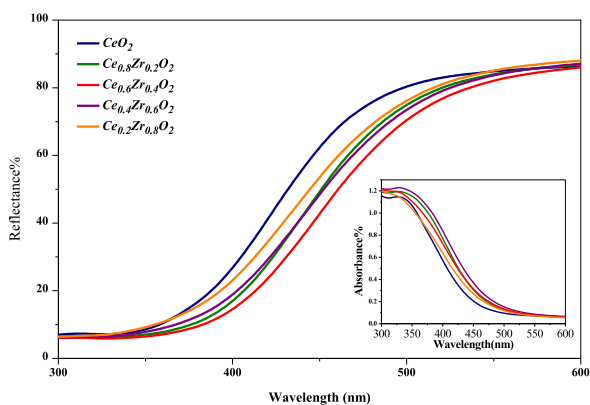


Fig. 10. UV–visible reflectance and absorbance spectra of the prepared samples.

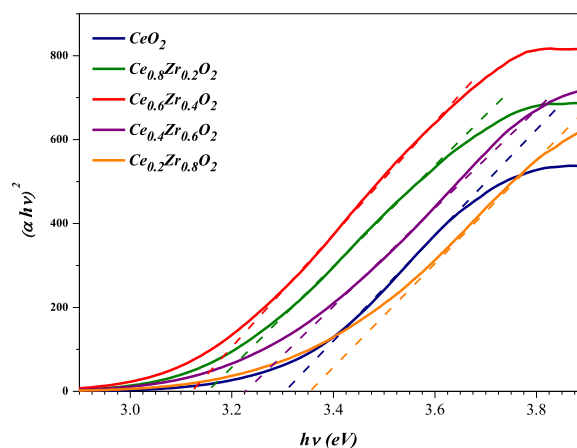


Fig. 11. Plot of $(\alpha h\nu)^2$ versus photon energy ($h\nu$).

carried out by a Konica Minolta CS2000 spectrophotometer.

3. Results and discussion

3.1. Thermogravimetric analysis (TGA)

The thermal behavior of the produced CeO₂ dried gel was analyzed using thermogravimetric analysis, in the range of room temperature to 800 °C, with a 5 °C/min heating rate. Fig. 3 Shows the TG curve of the gel and its corresponding derivative. The obtained TG curve can be

divided into three main mass loss parts. The first part, from room temperature to about 150 °C, is related to water evaporation. The second part, 150–350 °C, corresponds to decomposition of organic materials and the formation of the pyrochlore phase. The third part, from 350 °C to about 500 °C, is due to the formation of CeO₂ NPs. So the lowest calcination temperature needed to synthesize CeO₂ NPs was found to be about 500 °C.

Table 2
Colour coordinates and the band gap values of the samples.

Data name	L*	a*	b*	E _g (eV)
CeO ₂	98.86	-5.11	30.71	3.32
Ce _{0.8} Zr _{0.2} O ₂	94.90	-4.42	39.78	3.15
Ce _{0.6} Zr _{0.4} O ₂	94.40	-4.08	40.56	3.12
Ce _{0.4} Zr _{0.6} O ₂	96.12	-4.47	36.34	3.22
Ce _{0.2} Zr _{0.8} O ₂	94.94	-4.15	31.52	3.35
Ce _{0.8} Zr _{0.2} O ₂ (bulk) [20]	97.9	-2.2	12.1	3.00

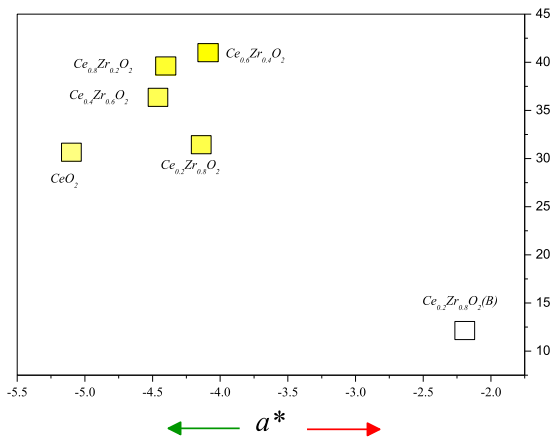


Fig. 12. Two dimensional coordinates of colour space a^*b^* of $Ce_{1-x}Zr_xO_2$ samples.

3.2. Structure analysis

The XRD patterns of $Ce_{(1-x)}Zr_xO_2$ NPs are given in Fig. 4. As these patterns show, no secondary phases are detected. The XRD patterns of the three prepared samples were analyzed by Fullprof software based on Rietveld refinements which are shown in Fig. 5. Our results revealed that the $Ce_{(1-x)}Zr_xO_2$ NPs with $x=0.0, 0.2, 0.4$ have cubic structures ($Fm-3m$ space group) and with $x=0.6, 0.8$ have tetragonal structures ($P42/nmc$), in accordance with JCPDS 34–0394 and JCPDS 80–2155, respectively [18,19]. Fig. 6 shows an enlarged image of the main diffraction peaks for $Ce_{(1-x)}Zr_xO_2$ NPs, in the range of $2\theta=27\text{--}32^\circ$. As shown in this figure, by increasing Zr concentrations, the main diffraction peak shifts toward higher angles since the ionic radius of Ce^{4+} (0.94 Å) is bigger than that of Zr^{4+} (0.84 Å) [20]. By increasing Zr concentrations, a decrease in the cubic lattice parameter (a) occurs due to smaller ionic radius of Zr^{4+} compared to Ce^{4+} , which is in accordance with Vegard's law [21]. A phase transition from cubic to tetragonal was observed with the increase of Zr concentrations. The XRD results indicated that the samples with $x=0.6$ and 0.8 have tetragonal phases, with higher c/a ratio in sample with $x=0.8$. These results are in good agreement with Yashima et al. [22]. However, it was observed that the phase transition between samples with $x=0.4$ and 0.6 is not sharp, which is confirmed by our Raman data analysis. The lattice parameters of the synthesized $Ce_{(1-x)}Zr_xO_2$ NPs are calculated, presented in Table 1. The average crystallite sizes of the samples were calculated using both the Scherrer formula ($D = \lambda l / \beta \cos \theta$) and size-strain plot (SSP) methods, accordingly we have:

$$(d\beta \cos \theta)^2 = \frac{K}{D} (d^2\beta \cos \theta) + \left(\frac{\varepsilon}{2}\right)^2 \quad (1)$$

where K is a constant which depends on the shape of the particles, β is the FWHM of the diffraction peaks, d is the plane's spacing, and θ is the diffraction peak angle [23]. To obtain the crystallite size and the lattice strain, the term $(d\beta \cos \theta)^2$ was plotted against $d^2\beta \cos \theta$. The crystallite size is calculated from the slope of linearly fitted data and the lattice strain from the y-intercept, as shown in Fig. 7. The results are given in Table 1. As it can be seen, the present strains in all samples are in the

order of micron. Also, with the increase of Zr in the samples with cubic phase, the average crystallite size decreases and the strain increases. However, in the samples with tetragonal structures the change in the average crystallite size is not remarkable.

According to the literature, the XRD patterns for ceria-zirconia compounds in cubic and tetragonal phases are almost similar, while their Raman spectra are completely different and therefore it would be easy to distinguish the present phases. Ceria with the cubic structure has only one Raman-active mode (F_{2g}), while the tetragonal zirconia has six Raman-active modes ($A_{1g}+2B_{1g}+3E_g$) [24]. The Raman spectra of the synthesized samples, which were obtained in the range of $200\text{--}700\text{ cm}^{-1}$ at room temperature, are presented in Fig. 8. The spectrum of pure CeO_2 shows a relatively high intensity band at 454 cm^{-1} , which can be attributed to the symmetry vibrational modes of oxygen ions surrounded by cerium ions. Aside from the F_{2g} mode in the sample with $x=0.2$ (Fig. 8), a broad band of low intensity at 596 cm^{-1} is detected which can be related to the presence of oxygen vacancies. A slight shift of the F_{2g} mode to higher wavenumbers, observed in Raman spectra of $Ce_{0.8}Zr_{0.2}O_2$ and $Ce_{0.6}Zr_{0.4}O_2$, can be due to the incorporation of Zr ions into the lattice of CeO_2 . In Raman spectra of $Ce_{0.4}Zr_{0.6}O_2$ and $Ce_{0.2}Zr_{0.8}O_2$, there are some other bands at $251, 303, 456, 577$ and 616 cm^{-1} , which are evidence for the presence of the tetragonal phases, confirming our XRD results.

Fig. 9 shows the TEM images and the corresponding size distribution histograms of the prepared CeO_2 and $Ce_{0.4}Zr_{0.6}O_2$ NPs. As it can be seen, the prepared NPs are distributed rather uniformly with the average particle size of about 9 and 8 nm for CeO_2 and $Ce_{0.4}Zr_{0.6}O_2$, respectively.

3.3. Optical analysis

The UV–vis diffuse reflectance spectra of the synthesized $Ce_{(1-x)}Zr_xO_2$ NPs, in the range of $300\text{--}600\text{ nm}$ wavelengths, are shown in Fig. 10, with the absorbance spectra presented in the appendix. It is observed that the absorption edge of the samples has a red-shift with the increasing Zr^{4+} concentrations. The optical band gaps (E_g) of the prepared samples were obtained using the UV–vis diffuse reflectance spectra and employing the Tauc relation as given by:

$$(\alpha h\nu)^{1/n} = C (h\nu - E_g) \quad (2)$$

Where C is a constant, $h\nu$ is the incident photon energy and α is the absorption coefficient obtained using the Kubelka–Munk function, $\alpha = (1 - R)^2 / 2R$, in which R is the reflectance [25]. In relation (2), n is 2 and $1/2$ for the samples with indirect and direct band gap, respectively. By plotting $(\alpha h\nu)^2$ versus $h\nu$ (Fig. 11), the band gaps were obtained which are given in Table 2. The value of the pure CeO_2 band gap is approximately 3.32 eV, due to direct electron transition from the valance band (O_{2p}) to the conduction band (Ce_{4f}) [19]. It is well known that the crystal structure, particle size and morphology affect the band gap value [26]. For the samples with cubic structures, the value of the band gap decreases by increasing Zr concentrations. Our results show that the value of the band gap of the samples with tetragonal structures are bigger than those with cubic phases, which can be related to the phase transition. For tetragonal samples the band gap value increases from 3.22 to 3.35 eV, which can be attributed to the increase in tetragonality. ZrO_2 has a wide band gap of 5 eV and can be reduced by replacing Zr^{4+} with Ce^{4+} , due to the presence of Ce_{4f} states in the gap [26,27]. Our optical results are in consistent with the other works [20,26].

3.4. Colorimetry

The CIE $L^*a^*b^*$ colour coordinates of the synthesized samples were measured, in which L^* is the brightness axis or the intensity of the pigments [black (0) to white (100)]; a^* axis represents the green-red

and b^* the blue-yellow, respectively. The results are presented in Table 2. The obtained CIE $L^*a^*b^*$ values indicate the bright yellow colour for our samples. The value of b^* shows that adding the dopant (Zr atoms) causes the colour change of nanoparticles to slightly more yellowish (Fig. 2). The negligible values of a^* correspond to the green tinge of the samples. The slight decrease of L^* values are related to the brightness reduction of the samples. The colour of all our synthesized NPs are yellow, while the colour of the $Ce_{0.8}Zr_{0.2}O_2$ bulk specimen is white with $L^*=97.9$, $a^*=-2.2$ and $b^*=12.1$, as reported by Vishnu et al. [20]. Our results showed that the $Ce_{0.6}Zr_{0.4}O_2$ nanopigment has the highest b^* value (40.56). Two dimensional coordinates of a b^* colour space of the prepared samples are given in Fig. 12.

4. Conclusions

$Ce_{(1-x)}Zr_xO_2$ NPs ($x=0.0, 0.2, 0.4, 0.6, 0.8$) were synthesized by a simple green sol-gel method, using gelatin biopolymer as the stabilization and polymerization agent. The produced gels were calcined at 600 °C. The XRD patterns confirmed the formation of the desired crystal structures without any extra unwanted peaks. The average crystallite size of the samples was calculated, using the Scherrer formula and SSP methods. Our XRD and Raman results revealed that the samples with $x=0.0, 0.2, 0.4$ are in cubic phase, while the samples with $x=0.6, 0.8$ have tetragonal phase. The TEM images indicated that the average particle size of the prepared NPs is about 8 nm. The energy band gaps of the samples were obtained from UV–vis spectra, according to the Kubelka–Munk method. It was found that the synthesized NPs have brilliant yellow colours which were derived by CIE- $L^*a^*b^*$ colour coordinates.

References

- [1] P. Cavalcante, M. Dondi, G. Guarini, M. Raimondo, G. Baldi, Colour performance of ceramic nano-pigments, *Dyes Pigments* 80 (2009) 226–232.
- [2] M. Patel, B. Bhanvase, S. Sonawane, Production of cerium zinc molybdate nano pigment by innovative ultrasound assisted approach, *Ultrason. Sonochem.* 20 (2013) 906–913.
- [3] S. Furukawa, T. Masui, N. Imanaka, New environment-friendly yellow pigments based on CeO_2 – ZrO_2 solid solutions, *J. Alloy. Compd.* 451 (2008) 640–643.
- [4] L.W. McKeen, *Fluorinated Coatings and Finishes Handbook: The Definitive User's Guide*, William Andrew, New York, 2015.
- [5] T. Masui, T. Honda, N. Imanaka, Novel and environmentally friendly (Bi, Ca, Zn) VO_4 yellow pigments, *Dyes Pigments* 99 (2013) 636–641.
- [6] S.K. Biswas, D. Dhak, A. Pathak, P. Pramanik, Chemical synthesis of environment-friendly nanosized yellow titanate pigments, *Mater. Res. Bull.* 43 (2008) 665–675.
- [7] K.J. Sreeram, R. Srinivasan, J.M. Devi, B.U. Nair, T. Ramasami, Cerium molybdenum oxides for environmentally benign pigments, *Dyes Pigments* 75 (2007) 687–692.
- [8] M. Jansen, H. Letschert, Inorganic yellow-red pigments without toxic metals, *Nature* 404 (2000) 980–982.
- [9] L.S. Kumari, P.P. Rao, A.N.P. Radhakrishnan, V. James, S. Sameera, P. Koshy, Brilliant yellow color and enhanced NIR reflectance of monoclinic $BiVO_4$ through distortion in VO_4^{3-} tetrahedra, *Sol. Energy Mater. Sol. Cells* 112 (2013) 134–143.
- [10] S. Furukawa, T. Masui, N. Imanaka, Synthesis of new environment-friendly yellow pigments, *J. Alloy. Compd.* 418 (2006) 255–258.
- [11] T. Masui, H. Tategaki, N. Imanaka, Preparation and characterization of SiO_2 – CeO_2 particles applicable for environment-friendly yellow pigments, *J. Mater. Sci.* 39 (2004) 4909–4911.
- [12] L.S. Kumari, P.P. Rao, S. Sameera, P. Koshy, Synthesis and optical properties of $Ce_{0.95}Pr_{0.05-x}M_xO_2$ ($M=Mn, Si$) as potential ecological red pigments for coloration of plastics, *Ceram. Int.* 38 (2012) 4009–4016.
- [13] R. Qing, W. Sigmund, Bi-functional $Ce_xZr_{1-x}O_2$ semiconductor nanoparticles with UV light switch, *J. Photochem. Photobiol. A: Chem.* 266 (2013) 55–63.
- [14] P. Bharali, P. Saikia, L. Katta, B.M. Reddy, Enhancement in CO oxidation activity of nanosized $Ce_xZr_{1-x}O_2$ solid solutions by incorporation of additional dopants, *J. Ind. Eng. Chem.* 19 (2013) 327–336.
- [15] D.H. Prasad, J.H. Lee, H.W. Lee, B.K. Kim, J.S. Park, Chemical synthesis and characterization of $Ce_xZr_{1-x}O_2$ powders by a modified sol gel method, *J. Ceram. Process. Res.* 10 (2009) 748–752.
- [16] C. Lin, C. Zhang, J. Lin, Phase transformation and photoluminescence properties of nanocrystalline ZrO_2 powders prepared via the Pechini-type sol-gel process, *J. Phys. Chem. C* 111 (2007) 3300–3307.
- [17] S. Rossignol, Y. Madier, D. Duprez, Preparation of zirconia–ceria materials by soft chemistry, *Catal. Today* 50 (1999) 261–270.
- [18] J.M. Hernández-Enríquez, R. Silva-Rodrigo, R. García-Alamilla, L.A. García-Serrano, B.E. Handy, G. Cárdenas-Galindo, A. Cueto-Hernández, Synthesis and Physico-Chemical Characterization of CeO_2/ZrO_2-SO_4 (2-) Mixed Oxides, *J. Mex. Chem. Soc.* 56 (2012) 115–120.
- [19] D. Tian, C. Zeng, H. Wang, H. Luo, X. Cheng, C. Xiang, Y. Wei, K. Li, X. Zhu, Performance of cubic ZrO_2 doped CeO_2 : first-principles investigation on elastic, electronic and optical properties of $Ce_{1-x}Zr_xO_2$, *J. Alloy. Compd.* 671 (2016) 208–219.
- [20] V. Vishnu, G. George, V. Divya, M. Reddy, Synthesis and characterization of new environmentally benign tantalum-doped $Ce_{0.8}Zr_{0.2}O_2$ yellow pigments: applications in coloring of plastics, *Dyes Pigments* 82 (2009) 53–57.
- [21] D. Mukherjee, B.G. Rao, B.M. Reddy, CO and soot oxidation activity of doped ceria: influence of dopants, *Appl. Catal. B: Environ.* 197 (2016) 105–115.
- [22] M. Yashima, H. Arashi, M. Kakihana, M. Yoshimura, Raman scattering study of cubic–tetragonal phase transition in $Zr_{1-x}Ce_xO_2$ solid solution, *J. Am. Ceram. Soc.* 77 (1994) 1067–1071.
- [23] A.K. Zak, W.A. Majid, M.E. Abrishami, R. Yousefi, X-ray analysis of ZnO nanoparticles by Williamson–Hall and size–strain plot methods, *Solid State Sci.* 13 (2011) 251–256.
- [24] V. Milman, A. Perlov, K. Refson, S.J. Clark, J. Gavartin, B. Winkler, Structural, electronic and vibrational properties of tetragonal zirconia under pressure: a density functional theory study, *J. Phys.: Condens. Matter* 21 (2009) 485404.
- [25] K.J. Sreeram, C.P. Aby, B.U. Nair, Synthesis and characterization of doped rare earth oxides for environmentally benign nontoxic reddish-yellow pigments, *Chem. Lett.* 37 (2008) 902–903.
- [26] H. Jiang, R.I. Gomez-Abal, P. Rinke, M. Scheffler, Electronic band structure of zirconia and hafnia polymorphs from the G W perspective, *Phys. Rev. B* 81 (2010) 085119.
- [27] C. Gionco, M.C. Paganini, E. Giamello, R. Burgess, C. Di Valentin, G. Pacchioni, Cerium-doped zirconium dioxide, a visible-light-sensitive photoactive material of third generation, *J. Phys. Chem. Lett.* 5 (2014) 447–451.